Published in final edited form as:
Nano Lett. 2010 May 12; 10(5): 1941–1949. doi:10.1021/nl101010m.

Rational Design and Synthesis of Freestanding Photoelectric Nanodevices as Highly Efficient Photocatalysts

Yongquan Qu[†], **Lei Liao**[†], **Rui Cheng**[‡], **Yue Wang**[†], **Yung-chen Lin**[‡], **Yu Huang**[‡,§], and **Xiangfeng Duan**[†,§,*]

[†] Department of Chemistry and Biochemistry, University of California, Los Angeles, CA 90095

[‡] Department of Materials Science and Engineering, University of California, Los Angeles, CA 90095

[§] California Nanosystems Institute, University of California, Los Angeles, CA 90095

Abstract

Photocatalysts are of significant interest for solar energy harvesting and conversion into chemical energy. However, the photocatalysts available to date are limited by either poor efficiency in the visible light range or insufficient photoelectrochemical stability. Here we report the rational design of a new generation of freestanding photoelectric nanodevices as highly efficient and stable photocatalysts by integrating a nanoscale photodiode with two redox catalysts in a single nanowire heterostructure. We show that a platinum-silicon-silver nanowire heterostructure can be synthesized to integrate a nanoscale metal-semiconductor Schottky diode encased in a protective insulating shell with two exposed metal catalysts. We further demonstrated that the Schottky diodes exhibited pronounced photovoltaic effect with nearly unity internal quantum efficiency, and that the integrated nanowire heterostructures could be used as highly efficient photocatalysts for a wide range of thermodynamically downhill and uphill reactions including photocatalytic degradation of organic dyes, reduction of metal ions and carbon dioxide using visible light. Our studies for the first time demonstrated the integration of multiple distinct functional components into a single nanostructure to form a standalone active nanosystem, and for the first time successfully realized a photoelectric nanodevice that is both highly efficient and highly stable throughout the entire solar spectrum. It thus opens a rational avenue to design and synthesize a new generation of photoelectric nanosystems with unprecedented efficiency and stability, and will impact broadly in areas including environmental remediation and solar fuel production.

Inorganic nanostructures such as nanodots, nanorods or nanowires are of considerable interest for solar energy harvesting and conversion.[1–20] Significant efforts have been placed on photovoltaic devices in which the photo-generated electrons and holes in nanostructures are transported to external circuits.[7–14] However, the difficulties in efficiently addressing individual nanostructures have prevented such materials from realizing their full potential for efficient solar energy harvesting. Photocatalysts mediated photoelectrochemical processes can utilize the photo-generated electrons and holes *onsite* for redox reactions.[1,2,21] This process enables the harness and conversion of solar energy into chemical energy *in-situ*, bypassing the most challenging problem associated with addressing individual nanostructures to transport electrical carriers to external circuits. However, the

*To whom the correspondence should be addressed. xduan@chem.ucla.edu.

Supporting Information Available. Experimental section, transmission electron microscopy images, optical spectrum of the xenon light used in the photocatalytic reaction, and method to calculate quantum efficiency of the photodiodes. This material is available free of charge via the internet at http://pubs.acs.org.

photocatalysts available to date are often limited by either poor efficiency in the visible light range or insufficient photo-electrochemical stability.[22–25]

An effective photocatalyst is usually comprised of three closely integrated elements: a semiconductor light harvesting antenna for solar energy absorption and two metal (or oxide) catalysts to facilitate the desired redox reactions.[26] Current photocatalysts are generally obtained by randomly loading metallic nanoclusters onto the surface of semiconductor particles. Oxide semiconductors (e.g. TiO_2) are typically explored here due to the limited electrochemical stability of other more conventional semiconductors (e.g. Si, GaAs, or CdS).[22,23,25] However, oxide semiconductors often suffer from having too large of a band gap for efficient absorption of solar irradiation and/or poor charge transport characteristics.[2,4] Despite considerable efforts,[3,5,27–29] most photocatalysts available to date only function in the ultraviolet (UV) or near UV regime. Significant challenges remain on developing a photocatalyst that is both efficient and robust enough in the visible range. The challenges include mismatch between semiconductor band gap and solar spectrum, inefficient charge separation, and deleterious semiconductor degradation side reactions that lead to material instability.[7–30]

Here we aim to rationally design and integrate multiple functional components into a single nanostructure to create a standalone photoelectric nanodevice that can serve as a highly efficient photocatalyst with high electrochemical stability. Specifically, we synthesize a Pt/n-Si/n^+-Si/Ag nanowire heterostructure to integrate a nanoscale metal-semiconductor Schottky photodiode (e.g. Pt/n-Si) with two metal catalysts (e.g. Ag and Pt) into a single nanowire heterostructure (Fig. 1). Here a Schottky diode is formed between Pt and n-Si due to a large work function difference, while a nearly Ohmic contact can be achieved between the heavily doped Si (n^+-Si) and Ag due to high doping concentration and small work function difference. The whole heterostructure nanowire device was encased in a protective insulating shell with the two metallic ends exposed for redox reactions, and each nanostructure functions as a complete standalone electrochemical cell. Specifically, photoexcitation of the semiconductor creates electron-hole pairs that quickly dissociate into separated electrons and holes due to the built-in electrical potential in the Pt/n-Si Schottky diode. The separated electrons and holes migrate in the opposite directions toward the two ends for desired reduction reaction on Ag and oxidation reaction on Pt, respectively.

The formation of these complex hetero-nanostructures as photocatalysts offers several key advantages. Firstly, nanoscale photodiode is created for efficient electron-hole separation; secondly, the one-dimensional morphology and insulating shell ensure the separated electrons and holes can only transport in the opposite directions toward two metal catalysts for desired reactions, and therefore minimizes non-productive recombination; thirdly, the encapsulation of the semiconductor portion in a protective insulating shell avoids direct electrochemical reactions on the semiconductor surface and therefore minimizes the deleterious side reactions that lead to semiconductor degradation and ensures the electrochemical stability of the whole system; and lastly, this ensured stability allows for flexible selection of semiconductors with desired band gaps for efficient visible light absorption.

This is in stark contrast to conventional semiconductor particle system with randomly loaded catalyst, in which the electron-hole separation and charge transport usually relies on diffusion with no clear directionality because the built-in potential is often not effectively established. Therefore, the recombination of electron hole pairs could dominate in the system with only small amount of carriers being able to diffuse to the surface of the semiconductor for redox reactions. Additionally, the directly exposed semiconductor surface with mobile charges can be highly susceptible to electrochemical reactions and degrade over

time. All these factors have limited the efficiency and stability of the conventional particle system.

Wafer-scale Si nanowire arrays were synthesized via a method combining colloidal lithography[31] with deep reactive ion etching (DRIE)[32–33] (Fig. 2a–g). Briefly, a highly doped (resistivity 0.01 ~ 0.02 Ω·cm) n-type Si (100) wafer with an 8-μm thick lightly doped epitaxial layer (resistivity 0.4 ~ 0.5 Ω·cm) and a 360 nm silicon oxide layer is used as the starting material (Fig. 2a). A close-packed monolayer of polystyrene (PS) spheres was formed on the surface of silicon oxide by a drop-casting method (Fig. 2b). The size of the PS spheres was reduced via controlled O_2 plasma etch, to transform the close-packed monolayer into a non-close-packed one (Fig. 2c). The exposed silicon oxide that was not protected by the PS spheres was then etched away, leaving a layer of patterned silicon oxide disks on the substrate as the etching mask for the subsequent DRIE process (Fig. 2d). After the DRIE process, vertical arrays of Si nanowires with controlled diameter and length were obtained (Fig. 2e). The sample was then immersed into chloroform followed by buffered oxide etchant (BOE) to remove the PS mask and any undesired residues deposited during the DRIE process (Fig. 2f). The sample was then heated under ambient conditions at 900 °C for 1 hour to result in a 50-nm silicon oxide shell on the nanowire surface (Fig. 2g).

The formation of Pt/Si heterojunctions involves selective drilling nanoholes into the Si nanowires from the top end and electrodeposition of Pt inside the nanoholes (Fig. 2h–m). To drill holes into the Si nanowires, the nanowires were first embedded in photoresist (Fig. 2h). The oxide layer at the top end of the nanowires was then exposed through oxygen plasma process and removed using RIE to expose the Si core (Fig. 2i). The Si core was subsequently partially etched away using a XeF_2 etcher to yield silicon oxide-protected Si nanowires with nanoholes of controlled depth (Fig. 2j). The sample was then immediately immersed into Pt electroplating solution for Pt deposition to form Pt/Si heterostructures (Fig. 2k).[34] The Pt-deposited sample was washed several times with hot acetone to remove photoresist and further cleaned by O_2 plasma to remove any remaining residues (Fig. 2l). The Pt/Si nanowire heterostructure could then be harvested and dispersed in solution by ultrasonication (Fig. 2m). Lastly, the Pt/Si/Ag photoelectric nanodevices can be obtained through self-catalyzed photoreduction and deposition of Ag on the silicon end (Fig. 2n).

Scanning electron microscopy (SEM) and transmission electron microscopy (TEM) were used to study the microstructure of the nanowire heterostructures. The close-packed polystyrene spheres were shrunk from the starting 1 μm diameter to ~700 nm, turning the close-packed monolayer (Fig. 3a) into a non-close-packed one (Fig. 3b). Controlled DRIE process was then performed to produce uniform vertically oriented Si nanowires with ~500 nm in diameter and ~10 μm in length with a 8 μm long n-Si and a ~2 μm long n^+-Si section (Fig. 3c,d). Top and side view of the Si nanowires after XeF_2 etching clearly shows that nanoholes with controlled depth can be drilled into the Si nanowires (Fig. 3e,f). Following the electrodeposition process, the SEM images clearly show that Pt was deposited inside the nanoholes to form a Pt/n-Si/n^+-Si nanowire heterostructure encased in silicon oxide shell (Fig. 3g,h). Figures 3i–k show the TEM images of a representative as-etched Si nanowire (Fig. 3i), a Si nanowire with a nanohole (Fig. 3j), and a Pt/Si heterojunction nanowire (Fig. 3k).

The photovoltaic properties of Pt/n-Si/n^+-Si nanowire photodiodes were characterized at individual nanowire level. To fabricate the device, the nanowire heterostructure was deposited on a Si substrate with a 100 nm silicon nitride layer, and Ti/Au (150 nm/50 nm) thin film electrodes were defined using e-beam lithography followed by e-beam evaporation to contact the Pt and n^+-Si section of the nanowire photodiode (Fig. 3l,m). The photovoltaic effect in the Pt/Si nanowire photodiode is clearly illustrated in the current-voltage (I–V) data

measured in dark and under one-sun irradiation (Fig. 3n). The I–V data obtained in dark shows clear current rectification effect with the consistent polarity, (i.e., the current can only flow through the device when Pt is positively biased), demonstrating the Schottky diode is formed as expected. The I–V data obtained under one-sun equivalent irradiation (100 mW/cm^2) shows clear photovoltaic effect with an open-circuit voltage V_{oc} of 0.30 V, a short-circuit current I_{sc} of 0.135 nA and a fill factor F_{fill} of 54 %. The apparent short-circuit current density J_{sc} calculated using the projected active area (Fig. 3m: 0.34 μm × 3.5 μm) is 11.2 mA/cm^2, which is much higher than the previous value of 3.5 mA/cm^2 reported for single Si nanowire with metal-semiconductor Schottky junction.[12] The photovoltaic power conversion efficiency η is 1.81 %, which is more than three times of the 0.5% value reported for Si p-i-n junction nanowire[13] and the 0.46% value reported for Si nanowires with metal-semiconductor junction.[12] It is important to note that only a very small portion of the photon was absorbed due to the small thickness of the Si nanowires. Considering the Si nanowire dimension and the Si absorption coefficient at variable wavelengths, we estimated that on average 20 % of total photons are absorbed by the Si nanowire (see supplementary information). Based on the short circuit current and the number of the absorbed photons, we obtained an average quantum efficiency (QE) of 88 % for the device in the entire spectral range (300–900 nm). Measurements on multiple devices show that all Pt/Si diodes exhibited photovoltaic effect with open circuit voltages of 0.15-0.3 V, power conversion efficiency of 1.0–2.0% and QE of 60–95%. These variations may be attributed to variable interface properties at the Pt-Si junction.

The vertical Pt/Si nanowire diodes were released from the wafer and dispersed in aqueous solution through a sonication process, in which the nanowires typically break at the nanowire-substrate interface. The Si core was exposed at the broken ends of the nanowires. In order to prevent the formation of a native silicon oxide layer on the exposed silicon surface that could block electron transfer in photocatalytic reactions, silver metal was immediately deposited on the Si end through a self-photocatalytic process (Fig. 2n). In this process, phototoexcitation of the Pt/Si photodiode created the electron-hole pairs which quickly separated into electrons and holes that travel in the two opposite directions toward the Si and the Pt ends, respectively. The electrons at the Si end reduced the Ag^+ in solution, leading to the deposition of Ag metal on the Si end. Another purpose for the metal deposition at the Si end is to integrate a selected metal catalyst that may facilitate desired photocatalytic reactions.

The photocatalytic deposition of Ag on the Si end was carried out by dispersing the nanowire diodes in 1 mM $AgNO_3$ aqueous solution. The wavelength of the simulated sunlight was cut off at 532 nm to avoid significant homogeneous photodecomposition of $AgNO_3$ in solution by the shorter wavelength light. The self-catalyzed photoreduction of Ag^+ to form Pt/Si/Ag nanowire photodiodes is illustrated in Figure 4a with the following reactions:

$$\mathrm{Pt/Si\ nanowire\ photodiode} \xrightarrow{h\nu} \mathrm{h^+ + e^-}$$
$$\mathrm{Cathode\ (silicon/silver): Ag^+ + e^- \rightarrow Ag}\quad E^0 = 0.79\ \mathrm{V}$$
$$\mathrm{Anode\ (platinum): 2H_2O + 4h^+ \rightarrow O_2 + 4H^+}\quad E^0 = -1.23\ \mathrm{V}$$

The redox potential of the total reaction is −0.21 V calculated from the equation:

$\Delta E = \Delta E_0 - 0.05916 \log \frac{[H^+](a_{O_2})^{0.25}}{[Ag^+]}$, when the $AgNO_3$ concentration is set at 1 mM with a solution pH of 6.75. The required potential is less than the open circuit voltage observed in the photodiodes, and the reaction can therefore effectively proceed forward.

TEM studies of the freshly released Pt/Si nanowire showed the broken Si end was pure silicon free of any obvious impurities (Fig. 4b). After light irradiation, small silver clusters (Fig. 4c) appeared at the end of the Si nanowires and continued to grow under irradiation. Eventually, silver metal covers the entire end of the Si nanowire to form a Pt/Si/Ag nanowire heterostructure (Fig. 4d). Energy dispersive X-ray (EDX) spectra (Fig. 4e–g) further confirmed three distinct sections of the heterostructure nanowire photodiode. It is important to note that electroless Ag deposition on fresh Si could also take place as the reaction has a potential of 1.70 V, considering the standard electrode potentials of Ag^+/Ag (0.79 V) and SiO_2/Si (−0.91 V) couples. In order to confirm the photoreduction of Ag^+ by the photodiode, a control reaction was carried out in dark for 3 hours using freshly released Pt/Si nanowires dispersed in the same $AgNO_3$ solution. TEM studies showed only very small silver clusters were observed at the end of the exposed Si (Fig. S1 a–b) in the control reaction, in contrast to the large silver particles obtained with irradiation for the same period of time (Fig. 4d). In the electroless deposition, the required electrons for reducing Ag^+ was supplied by the oxidation of silicon atoms on the surface, which in turn generated a silicon oxide layer. With ongoing reaction, the silicon oxide layer would become too thick to allow efficient electron transfer, and therefore limited the continued growth of Ag particles. Hence only small Ag particles were observed. On the other hand, the electrons needed in photoreduction of the Ag^+ were continuously supplied by the photogeneration and separation of electron-hole pairs, which could sustain the continuous growth of the Ag particles. To further confirm the effect of Pt-Si diode in the self-catalyzed deposition of Ag, we have also carried out a control reaction using freshly released Si nanowires without Pt deposition step. No obvious silver nanoparticles were observed on either ends of the Si nanowires after 3 hours of light irradiation in 1 mM $AgNO_3$ solution (Fig. S1 c). These results clearly demonstrated the essential role of the Pt/Si nanowire photodiodes in the photocatalytic reduction of silver in our system.

Based on the total mass of the silver particle produced at the Si end, the total irradiation flux and the estimated absorption, it was possible to estimate the QE of the silver photoreduction process (the number of Ag^+ reduced vs. the number of photons absorbed). Our estimation gave an apparent QE of 0.007%, which was many orders of magnitude lower than that of the photovoltaic device described in Figure 3n. This difference may be attributed to a number of factors. First, the freshly released silicon may form a thin layer of silicon oxide as soon as they are exposed to environment and dispersed in water, which can hinder the efficiency of the charge transport from the photodiode to Ag^+; therefore, the initial nucleation of silver cluster is slow and accelerates as silver clusters are nucleated and directly deposited on Si. On the other hand, with the proceeding of the experiment, the solution pH decreases, which can significantly increase the required redox potential $\Delta E=\Delta E_0 - 0.05916\log\frac{[H^+](a_{O_2})^{0.25}}{[Ag^+]}$, and therefore decelerates the photoreduction reaction rate. Therefore, we would expect an overall acceleration and then saturation in the photoreduction reaction.

The reaction process can be effectively monitored by the evolution of the pH value (proton concentration $[H^+]$) of the reaction solution or the size of the Ag nanoparticle on the Si end. Importantly, plot of proton concentration of the reaction solution with Pt/Si nanowire as a function of irradiation time showed that the proton concentration increased superlinearly at the beginning and then saturated at pH~5.39 (Fig. S2), suggesting an accelerating stage followed by a decelerating stage in the reaction, as expected. In contrast, the solution in a control reaction without Pt/Si nanowire also showed pH change but to a much smaller degree (Fig. S2), which can be attributed to a small amount of homogeneous decomposition of $AgNO_3$. Subtracting the $[H^+]$ change in the control reaction, the net change of $[H^+]$ (Fig. 4h, black) clearly showed three distinct reaction stages: slower nucleation, fast growth and

then saturation. Similarly, the size of the largest Ag nanoparticle on the Si end also showed a similar acceleration and saturation effect (Fig. 4i). Both the proton concentration and silver volume indicated a saturation that started around 3 hours at pH~5.39. The required redox potential $\Delta E=\Delta E_0 - 0.05916\log\frac{[H^+](a_{O_2})^{0.25}}{[Ag^+]}$ at this point was −0.29 V, close to the built-in potential by the best nanowire photovoltaic cell. Therefore, at this point, the photodiode could no longer supply electrons that were energetic enough to drive the reaction forward. Therefore, the apparent QE of the photocatalytic effect was limited due to the two competing factors that limited the rate of silver reduction. This trend was further confirmed by light irradiation of the re-dispersed Pt/Si/Ag nanowire photodiodes in 1 mM $AgNO_3$ solution. The plot of the net change of $[H^+]$ versus the reaction time only showed a fast reaction rate at the beginning and a saturation after 2 hours irradiation (Fig. 4h, red triangle), without the initial slow nucleation stage observed in the reaction of Pt/Si nanowire photodiodes (Fig. 4h, black square). The QE of these photodiodes in the photocatalytic reduction of Ag^+ can be derived from the steepest slope in Figure 4h, and 4i, which gives a QE of 0.0012% and 0.039%, respectively. The higher value obtained from the silver volume than that from the $[H^+]$ is reasonable, considering the former represents the QE in the best photodiode and the later represents the average QE of all photodiodes. Overall, the QE of the silver photoreduction reaction is rather low, which may also be partly attributed to substantial overpotential for the water oxidation reaction and oxygen evolution process, and may be improved by coupling additional catalyst to reduce this overpotential.[35]

With the self-catalyzed photodeposition of Ag on the exposed Si end, we obtain a Pt/n-Si/n^+-Si/Ag heterojunction in a single nanowire, in which the platinum is in contact with the lightly doped n-silicon to form a Schottky photodiode, and Ag in contact with the highly doped n^+-Si with a nearly Ohmic contact. The entire device is encased in a silicon oxide shell except for the Pt and Ag ends. Thus, a nanoscale photodiode and two distinct metal catalysts are integrated into a single nanostructure with an insulating protective shell. This nanostructure can function as a standalone photoelectric nanodevice that can be used for highly efficient photocatalytic reactions while maintaining high electrochemical stability with minimal semiconductor degradation. The formation of Pt/Si/Ag heterojunction photoelectric nanodevices thus opens exciting opportunities for a wide range of photocatalytic reactions. To this end, we have explored such photoelectric nanodevices to facilitate both thermodynamically downhill and uphill reactions, such as the photocatalytic degradation of organic compounds (e.g. indigo carmine, IC) and photocatalytic reduction of carbon dioxide.

The photocatalytic degradation of organic compounds is a thermodynamically downhill reaction, and is of significance in waste treatment of organic pollutants. Under light irradiation, the electron-hole pairs are generated in the photodiode and then quickly separated. The holes can be captured by water, to produce reactive oxygen species (ROS), such as hydroxyl radicals ($OH^\bullet$), superoxide ($O_2^{\bullet-}$), singlet oxygen ($^1O_2$), and peroxide (H_2O_2) that act as strong oxidants.[36] The ROS are known as nonselective oxidizing agents for many organic pollutants. They can oxidize IC into CO_2, H_2O, HNO_3 and sodium sulfate. The reactions are listed as following.

$$\text{Pt/Si/Ag nanowire photodiode} \xrightarrow{h\nu} h^+ + e^-$$
$$\text{Cathode: } O_2 + 4H^+ + 4e^- \rightarrow 2H_2O$$
$$\text{Anode: } h^+ + H_2O \rightarrow \text{ROS} + H^+$$
$$\text{ROS} + \text{indigo carmine} \rightarrow \text{intermediates} \rightarrow CO_2 + H_2O + HNO_3 + \text{sodium sulfate}$$

To study the photocatalytic degradation reaction, 10 ml of 100 μM IC solution containing 1.2×10^8 Pt/Si/Ag nanowire diodes was irradiated under a xenon light for 45 minutes, and the change of IC concentration was monitored as a function of time. Our studies showed that 64.5% of IC molecules were degraded within the first 5 minutes with the aid of Pt/Si/Ag photocatalysts (Fig. 5a). In contrast, less than 2% of the IC was degraded with the same irradiation conditions without the photodiode photocatalysts. The apparent QE of the reaction was calculated to be ~ 2.93 % based on the first 5 min of the reaction (see supplementary information). We note that the QE varied significantly with IC concentration. At higher IC concentration (10 mM), a QE of 41.9 % could be achieved. Similar trend was also observed previously.[37] The IC concentration dependence of QE may be attributed to the variable capture efficiency of the ROS by IC dye. Low IC concentration led to lower capture efficiency, which in turn resulted in an apparently lower calculated QE in the photocatalytic reactions.

We have also studied the spectral response of the QE of the photocatalytic degradation reaction with Pt/Si/Ag nanowire photodiodes (Fig. 5b). Importantly, the QE is nearly constant at around 45.0 % throughout the whole spectral regime, which is consistent with the overall QE value of 41.9 % obtained with the white light irradiation. These results highlight that the Pt/Si/Ag nanowire photodiodes can be used as photocatalysts for photocatalytic reactions using visible or even near IR irradiations, in contrast to TiO_2 based photocatalysts that are only active in the UV or near UV region.

It is also important to evaluate the photocatalytic stability of the photocatalysts. To this end, we have compared our Pt/Si/Ag diode photocatalysts with TiO_2 photocatalysts, one of the most widely studied and stable photocatalysts. A recent study showed the activity of TiO_2 photocatalysts in IC degradation reaction degraded by 10% after 10 cycles of photocatalytic reactions.[38] In contrast, under the same conditions, the photocatalytic activity of Pt/Si/Ag diodes remained essentially constant over 30 cycles of reactions (Fig. 5c), demonstrating the exceptional stability of Pt/Si/Ag nanowire photodiodes in photocatalytic reactions. This improved stability can be attributed to the integrated protective oxide shell, which insulates the semiconductor from any kind of photoelectrochemical degradation.

It is possible to explore the Pt/Si/Ag diodes to catalyze thermodynamically uphilll reactions. To this end, we have explored the diodes for the CO_2 reduction reaction, in which H_2 is used to reduce CO_2 into small organic compounds such as formic acid, with an extra potential of 0.11 V. The reactions are listed as following:

$$\text{Pt/Si/Ag nanowire photodiode} \xrightarrow{h\nu} h^+ + e^-$$
$$\text{Cathode (silver):} CO_2 + 2H^+ + 2e^- \rightarrow HCOOH \quad E^0 = -0.11\ \text{V}$$
$$\text{Anode (platinum):} H_2 + 2h^+ \rightarrow 2H^+ \quad E^0 = 0\ \text{V}$$

The reaction was carried out by irradiating a reaction solution with a xenon light while bubbling both CO_2 and H_2 into the solution containing the Pt/Si/Ag diodes. The amount of the products (formaldehyde, HCHO and formic acid, HCOOH) was determined by the Nash reagent[39,40] with a 412 nm absorption peak. Out studies showed that the main product was formic acid, with only a trace amount of formaldehyde. Therefore, only formic acid is considered here. The photocatalytic reduction reaction was carried out in 40 ml of reaction solution containing 6×10^7 well dispersed Pt/Si/Ag nanowire photodiodes at a flow rate 300 sccm for CO_2 and H_2. At such a fast gas flow rate, the products could be carried out by the gas flow and tend to saturate quickly in the reaction vessel. In order to capture all the products carried out by the gas flow, four ice-cold water traps were connected to the reaction flask to collect the product. Figure 5d shows the plot of the total amount of photoreduced

formic acid vs. the reaction time. The plot shows a quick increase of formic acid at the beginning in the first 30 minutes followed by a slower linear increase. In this reaction, the concentration of the product, formic acid, saturated at 6.0 mM in reaction flask, with a redox potential $\Delta E=\Delta E_0 - \frac{0.05916}{2}\log\frac{[HCOOH]}{a_{H_2} \times a_{CO_2}}$ of −0.062 V. Therefore, the reaction conditions were almost identical for the continued reaction, leading to a near linear increase of the amount of formic acid in continued reaction. A total of 0.357 mmol formic acid was generated within 10 minutes. The calculated QE was about 19.9 %. We note this QE is much higher than Ag^+ reduction reaction, which may be attributed to the considerably smaller required redox potential (~0.06 V for CO_2 reduction versus ~0.2–0.3 V for Ag^+ reduction).

In conclusion, we have designed and synthesized a novel metal-semiconductor-metal heterostructure that integrates a nanoscale metal-semiconductor Schottky photodiode (e.g. Pt/n-Si) with two metal catalysts (e.g. Ag or Pt) in a single nanowire. The Pt/Si/Ag nanowire heterostructures can function as stand-alone photoelectric nanodevices with exceptional photocatalytic properties for both thermodynamically downhill and uphill reactions. Our studies for the first time demonstrated the integration of multiple distinct components into a single nanostructure to form a standalone functional nanosystem, and for the first time successfully realized a photoelectric nanodevice that is both highly efficient and highly stable throughout the whole solar spectrum. It thus opens a new avenue to rational design and synthesis of a new generation of photoelectric nanosystems with unprecedented efficiency and stability. Future work to explore larger band gap semiconductors (e.g. CdS) or tandem structures can lead to photoelectric nanodevices with larger built in potential for important photocatalytic reactions including direct water splitting. It can therefore impact broadly in areas including environmental remediation and solar fuel production. Lastly, we note that the current synthetic approach to the Pt/Si/Ag photoelectric nanodevices is rather complex and could be costly in practical applications. Nonetheless, our studies demonstrate that this rationally designed photoelectric nanosystem represents a much more efficient and stable photocatalyst system, and point out a clear pathway to a new generation of photocatalysts. Alternative approaches (e.g. wet chemical etch[41,42], chemical vapor deposition[43] and solution chemistry synthesis[44,45]) may be explored for the bulk synthesis of such complex heterostructures with much reduced cost.

Supplementary Material

Refer to Web version on PubMed Central for supplementary material.

Acknowledgments

We acknowledge support by the NIH Director’s New Innovator Award Program, part of the NIH Roadmap for Medical Research, through Grant 1DP2OD004342-01. Y.H. acknowledges support from the Office of Naval Research under award N00014-08-1-0985. We acknowledge Electron Imaging Center for Nanomachines (EICN) at UCLA for support for TEM, Nanoelectronics Research Facility at UCLA for support of device fabrication.

References

1. Bard AJ. Science. 1980; 207:139–144. [PubMed: 17809089]
2. Goetzberger A, Hebling C, Schock HW. Mater Sci Engineer R. 2003; 40:1–46.
3. Hagfeldt A, Gratzel M. Acc Chem Res. 2000; 33:269–277. [PubMed: 10813871]
4. Gratzel M. Nature. 2001; 414:338–344. [PubMed: 11713540]
5. Law M, Greene LE, Johnson JC, Saykally R, Yang PD. Nature Mater. 2005; 4:455–459. [PubMed: 15895100]
6. Hayden O, Agarwal R, Lieber CM. Nature Mater. 2006; 5:352–356. [PubMed: 16617344]

7. Lewis NS. Science. 2007; 315:798–801. [PubMed: 17289986]
8. Gur I, Fromer NA, Geier ML, Alivisatos AP. Science. 2005; 310:462–465. [PubMed: 16239470]
9. Luque A, Marti A, Nozik AJ. MRS Bulletin. 2007; 32:236–241.
10. Tian BZ, Zheng XL, Kempa TJ, Fang Y, Yu NF, Yu GH, Huang JL, Lieber CM. Nature. 2007; 449:885–889. [PubMed: 17943126]
11. Yang C, Barrelet CJ, Capasso F, Lieber CM. Nano Lett. 2006; 6:2929–2934. [PubMed: 17163733]
12. Kelzenberg MD, Turner-Evans DB, Kayes BM, Filler MA, Putnam MC, Lewis NS, Atwater HA. Nano Lett. 2008; 8:710–714. [PubMed: 18269257]
13. Kempa TJ, Tian BZ, Kim DR, Hu JS, Zheng XL, Lieber CM. Nano Lett. 2008; 8:3456–3460. [PubMed: 18763836]
14. Tian B, Kempa TJ, Lieber CM. Chem Soc Rev. 2009; 38:16–24. [PubMed: 19088961]
15. Tada H, Mitsui T, Kiyonaga T, Akita T, Tanaka K. Nature Mater. 2006; 5:782–786. [PubMed: 16964238]
16. Costi R, Saunders AE, Elmalem E, Salant A, Banin U. Nano Lett. 2008; 8:637–641. [PubMed: 18197720]
17. Dukovic G, Merkle MG, Nelson JH, Hughes SM, Alivisatos AP. Adv Mater. 2008; 20:4306–4311.
18. Menagen G, Macdonald JE, Shemesh Y, Popov I, Banin U. J Am Chem Soc. 2009; 131:17406–17411. [PubMed: 19894717]
19. Carbone L, Jakab A, Khalavka Y, Sonnichsen C. Nano Lett. 2009; 9:3710–3714. [PubMed: 19813756]
20. Schierhorn M, Boettcher SW, Kraemer S, Stucky GD, Moskovits M. Nano Lett. 2009; 9:3262–3267. [PubMed: 19705806]
21. Kamat PV. J Phys Chem C. 2007; 111:2834–2860.
22. Manassen J, Cahen D, Hodes G, Sofer A. Nature. 1976; 263:97–100.
23. Tsubomura H, Matsumura M, Nakatani K, Yamamoto K, Maeda K. Solar Energy. 1978; 21:93–98.
24. Zhang HJ, Guohua C, Bahnemann DW. J Mater Chem. 2009:5089–121.
25. Kudo A, Miseki Y. Chem Soc Rev. 2009; 38:253–278. [PubMed: 19088977]
26. Bard AJ. J Photochem. 1979; 10:59–75.
27. Maier CU, Specht M, Bilger G. Int J Hydrogen Energy. 1996; 21:859–864.
28. Li D, Haneda H, Hishita S, Ohashi N. Chem Mater. 2005; 17:2596–2602.
29. Robel I, Subramanian V, Kuno M, Kamat PV. J Am Chem Soc. 2006; 128:2385–2393. [PubMed: 16478194]
30. Lewis NS. Nature. 2001; 414:589–590. [PubMed: 11740538]
31. Yang SM, Jang SG, Choi DG, Kim S, Yu HK. Small. 2006; 2:458–475. [PubMed: 17193068]
32. Morton KJ, Nieberg G, Bai SF, Chou SY. Nanotechnology. 2008; 19:345301.
33. Cheung CL, Nikolic RJ, Reinhardt CE, Wang TF. Nanotechnology. 2006; 17:1339–1343.
34. Zhao GY, Xu CL, Guo DJ, Li H, Li HL. Appl Surf Sci. 2007; 253:3242–3246.
35. Kanan MW, Nocera DG. Science. 2008; 321:1072–1075. [PubMed: 18669820]
36. Rajeshwar K, Osugi ME, Chanmanee W, Chenthamarakshan CR, Zanoni MVB, Kajitvichyanukul P, Krishnan-Ayer R. J Photochem Photobiol C. 2008; 9:171–192.
37. Subramani AK, Byrappa K, Ananda S, Rai KML, Ranganathaiah C, Yoshimura M. Bull Mater Sci. 2007; 30:37–41.
38. Costa LL, Prado AGS. J Photochem Photobiol A. 2009; 201:45–49.
39. Nash T. Biochem J. 1953; 55:416–421. [PubMed: 13105648]
40. Erikson JM, Biggs HG. J Chem Edu. 1973; 50:631–632.
41. Peng KQ, Yan YJ, Gao SP, Zhu J. Adv Funct Mater. 2003; 13:127–132.
42. Qu YQ, Liao L, Li YJ, Zhang H, Huang Y, Duan XF. Nano Lett. 2009; 9:4539–4543. [PubMed: 19807130]
43. Patolsky F, Zheng GF, Lieber CM. Nature Protocols. 2006; 1:1711–1724.
44. Holmes JD, Johnston KP, Doty RC, Korgel BA. Science. 2000; 287:1471–1473. [PubMed: 10688792]

45. Pena DJ, Mbindyo JKN, Carado AJ, Mallouk TE, Keating CD, Razavi B, Mayer TS. J Phys Chem B. 2002; 106:7458–7462.

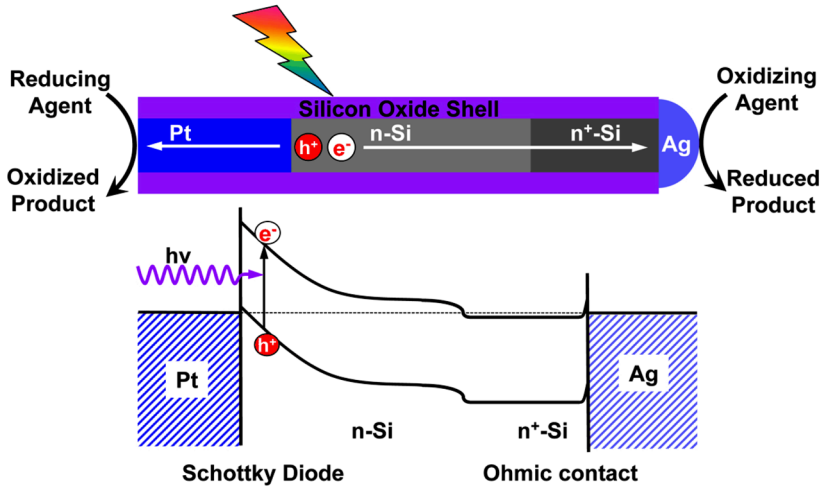

Figure 1.

Schematic illustration and band diagram of a rationally designed metal-semiconductor-metal photoelectric nanodevice as highly efficient photocatalysts. Here a Pt/n-Si/n^+-Si/Ag heterostructure is created in a single nanowire to integrate a nanoscale metal-semiconductor Schottky photodiode (Pt-Si) encased in a protective insulating shell with two exposed metal catalysts (Pt, Ag). The photoexcitation of the semiconductor creates electron-hole pairs that quickly dissociate into separated electrons and holes, which migrate in the opposite directions toward the two ends for desired reduction reaction on Ag and oxidation reaction on Pt, respectively. This nanostructure can function as a standalone photoelectric nanodevice that can be used for highly efficient photocatalytic reactions while maintaining high electrochemical stability with minimal semiconductor degradation.

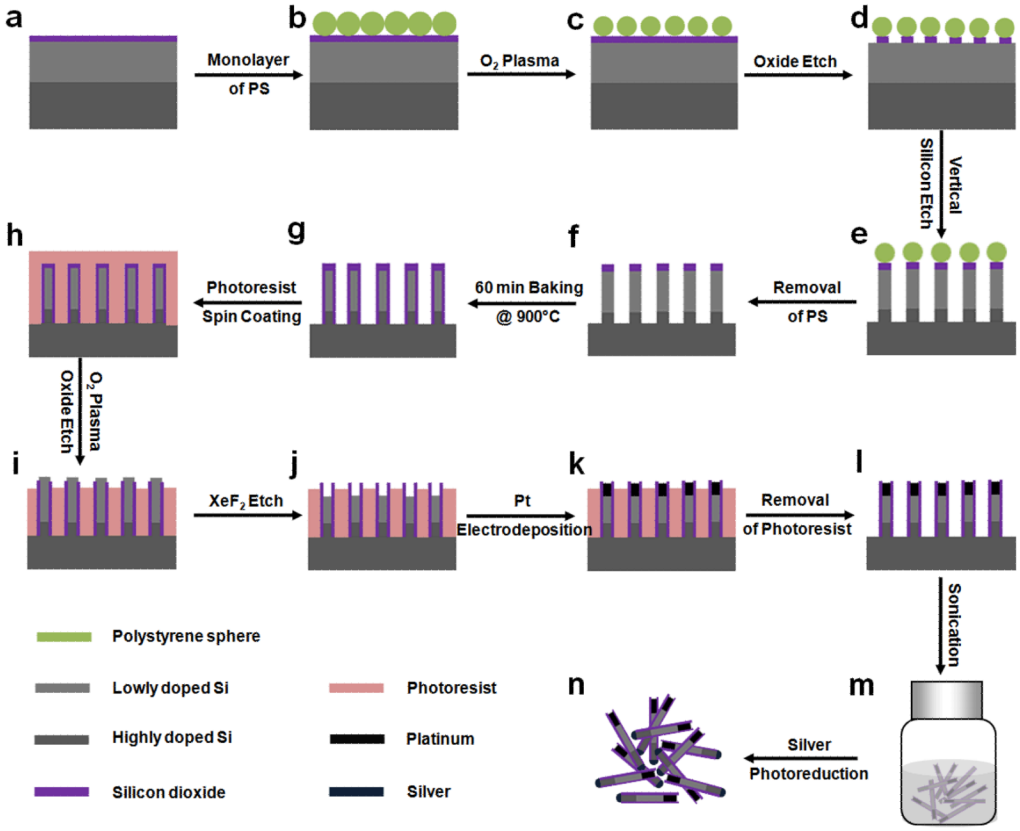

Figure 2.

Schematic illustration of the synthesis of Pt/Si/Ag nanowire photodiodes. (a) The starting n/n^+ silicon wafer with a 360 nm silicon oxide. (b) Formation of close-packed monolayer of polystyrene (PS) spheres by a drop casting method. (c) Formation of non-close-packed monolayer of PS spheres by O_2 plasma. (d) Formation of the patterned DRIE etching-mask containing PS spheres and the underneath silicon oxide discs obtained from using an AOE oxide etching recipe. (e) Using DRIE to obtain vertical Si nanowire arrays. (f) Removal of PS spheres and the residue in chloroform and hydrofluoric acid solution. (g) Formation of silicon oxide shell on Si nanowires by baking sample under ambient conditions at 900 °C for 60 min. (h) Spin coating of photoresist AZ 5214 as a protecting layer for the substrate. (i) Exposure of the Si core of the silicon oxide-encased Si nanowires through an O_2 plasma process followed by oxide dry etching. j. Drilling of the nanoholes in the Si nanowires by XeF_2 dry etching. (k) Pt electrodeposition. l, Removal of photoresist AZ 5214. m, Release of Pt/Si nanowires into solvent through sonication. (n) Self-catalyzed photoreduction of silver by irradiation on freshly released Pt/Si nanowires in $AgNO_3$ aqueous solution.

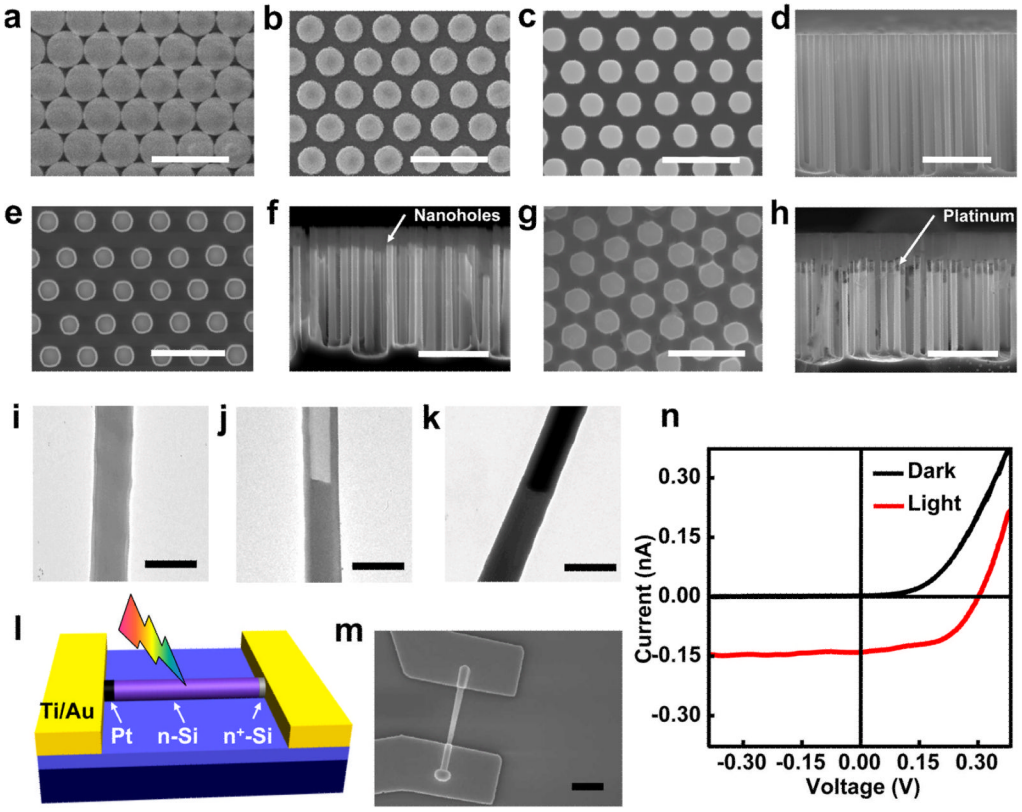

Figure 3.

Structural characterization of the nanostructures and photovoltaic performance of individual Pt/Si nanowire photodiodes. (a) SEM image of monolayer of close-packed PS spheres. (b) SEM image of monolayer of non-close-packed PS spheres. (c d) SEM images of top view and cross-sectional view of the as-etched Si nanowires. (e, f) SEM images of top view and cross-sectional view of Si nanowires with nanoholes. (g,h) SEM images of top view and cross-sectional view of Pt-filled Si nanowires. i, TEM image of a dry etched Si nanowire. (j) TEM image of a Si nanowire with a nanohole. (k) TEM image of a Pt/Si nanowire heterojunction. (l) Schematic illustration of the fabricated device of individual Pt/Si nanowire photodiode. (m) SEM image of a Pt/Si nanowire device. To make the device, the Pt section was controlled to be ~3 μm. The spherical tip at the Pt end is resulted from intentionally excessive electrodeposition of Pt. (n) I–V data obtained in dark (black) and under one-sun irradiation (red). Scale bar is 5 μm for d, f, and h, 2 μm for a, b, c, e, g and m, and 700 nm for i–k.

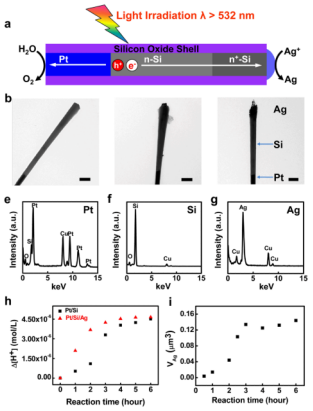

Figure 4.

Formation of Pt/Si/Ag nanowire photodiodes. (a) Schematic illustration of self-catalyzed silver photoreduction. Only long wavelength light (λ>532 nm) were used here to avoid significant homogeneous photodecomposition of $AgNO_3$. (b) Pt/Si nanowire before silver photoreduction. (c) Pt/Si nanowires dispersed in 1mM $AgNO_3$ solution with 0.5 hour light irradiation. (d) Pt/Si/Ag nanowire diode obtained after 3 hours light irradiation in 1mM $AgNO_3$ solution. The scale bars in b–d is 700 nm. (e–g) EDX spectra of three distinct sections (Pt, Si and Ag) of a nanowire photodiode. (h) Plot of the net change of proton concentration with the reaction time. Black square (red triangle) represent the result obtained from 2.2×10^7 Pt/Si (Pt/Si/Ag) photodiodes in 6 ml of 1 mM $AgNO_3$ solution. (i) Plot of the largest total silver volume with the reaction time.

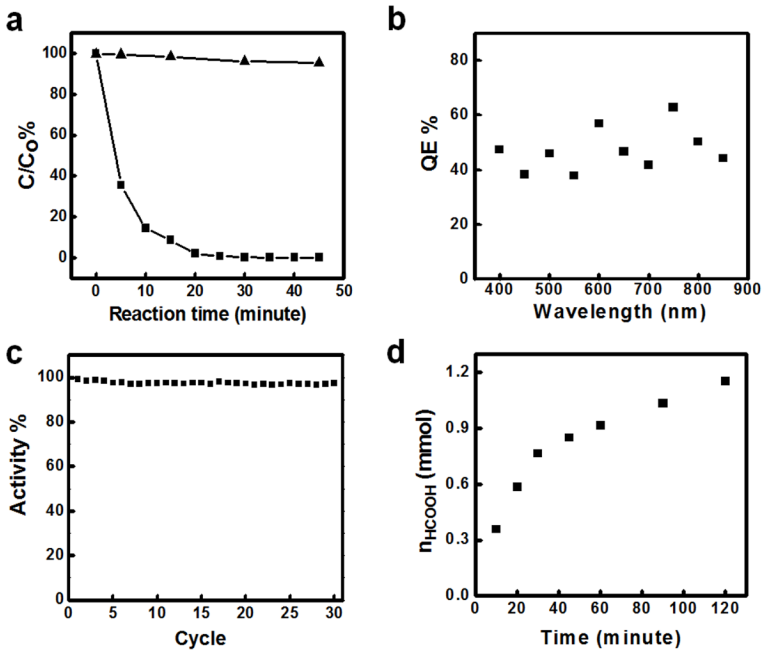

Figure 5.

Photocatalytic properties of Pt/Si/Ag photodiode. (a) Photodegradation of indigo carmine (IC) with 1.2×10^8 Pt/Si/Ag photodiodes dispersed in 10 ml of 100 μM IC aqueous solution. The degradation was characterized by the ratio of measured concentration to its original concentration. The triangles represent the photodegradation reaction of IC without photodiodes. The squares represent the same photodegradation reaction of IC with Pt/Si/Ag photodiodes. (b) Estimated QE of Pt/Si/Ag nanowire photodiodes within visible light range. For the reaction, 6×10^8 Pt/Si/Ag nanowire photodiodes were dispersed in 2 ml of 10 mM IC aqueous solution. The mixture was exposed to a selected wavelength for 30 minutes for each wavelength. (c) Photocatalytic stability of the Pt/Si/Ag photodiodes in the IC degradation reaction. The experiment is carried out with 2.0×10^7 diodes dispersed in 1 ml of 50μM IC solution with the initial 98% degradation of the IC dye. (d) Plot of the total amount of formic acid with respect to the reaction time. In this reaction, 300 sccm CO_2 and 300 sccm H_2 were bubbled through 40 ml of 0.04 M Na_2CO_3 solution containing 1×10^8 Pt/Si/Ag nanowire photodiodes.